Electromagnetic Characterisation of a Short-Stroke Ferromagnetic Actuator Technical Note

Bowen Zhang, *1975667* and Weifeng Du, *1975663*

***Abstract*—The electromagnetic actuators are widely used in automotive, industrial automation and protection system [1]. In this article, a model was built using MATLAB and FEMM in order to analyse the characterization of an actuator and the comparison between different analyzing methods is made. The principle of a short-stroke ferromagnetic actuator is discussed and 4 different modelling approaches used to model the actuator are compared. In addition, the resistance, inductance of the actuator and force imparted on mover of the actuator are discussed in this article. It has been found that FEMM simulation tools using non-linear core produces the most accurate result.**

I. Introduction

This technical note incorporates the calculations of the winding resistance, winding inductance of a Short-Stroke Ferromagnetic Actuator depicted in Fig. 1 and the finding on the force imparted on the Armature. Four different modelling approaches are used with the intention of finding the inductance of the actuator and force imparted on the mover (i.e. analytical equivalent circuit without considering air-gap fringing, analytical equivalent circuit with air-gap fringing, FEMM with linear materials and FEMM with non-linear materials [2]). The modelling method discussed in this technical note is Finite Element Method Magnetic (FEMM), which plays a critical role in discipline of electromagnetic field. The Finite Element Method(FEM) emerges in different disciplines such as biology [3], civil engineering [4] and dynamics [5] MATLAB and FEMM are used for more precise and faster calculations.

II. Winding Resistance

A. The Winding resistance calculated using voltage and current measured by FEMM

FEMM and MATLAB can be readily used to calculate the winding resistance. This can be achieved by using command *mo_getcircuitproperties()* to calculate the current I and voltage V in the coil. Then the resistance could be found using (1)

$$R_w = \frac{V_w}{I_w} \tag{1}$$

According to the data collected from FEMM model, the voltage and current on a single coil is $V_w = 0.1066\,\mathrm{V}$ and $I_w = 10\,\mathrm{A}$, the resistance could be calculated using (1), which yields the single winding resistance R_w=10.66 $m\Omega$.

B. The Winding resistance calculated using effective length measured by FEMM

Another approach is to use (2) to calculate the effective length l_w. Thus, it would be possible to calculate the R_w with the definition of resistance described in (3) [6]

$$l_w = \frac{V_w}{A_w} \tag{2}$$

$$R_w = \frac{N l_w}{\sigma((k_{PF})A_w)/N} \tag{3}$$

The volumeof coil V_w and the area of the cross-section A_w could be measured by the FEMM, which are $V_w = 1.29 \times 10^{-5}\,m^3$ and $A_w = 6.48 \times 10^{-4}\,m^2$. Substitute them into (2), the effective length l_w could be found, which is $l_w = 2\,\mathrm{cm}$. Then if substitute $l_w = 2\,\mathrm{cm}$, $N = 100\,\mathrm{turns}$, $\sigma = 58\,\mathrm{MS/m}$, $k_{PF} = 0.6$ and $A_w = 6.48 \times 10^{-4}\,m^2$ into (3), it is readily to find the resistance of a half of a winding is $R_{halfwinding} = 8.896\,m\Omega$. Both two windings comprise 2 of the half winding. Thus, the total resistance of one winding is $R_w = 17.79\,m\Omega$.

C. The Winding resistance calculated using CAD model

However, the FEMM model used in simulation is a 2D model, which omits more than a half of the coil in simulation. In the light of this, as shown in Fig. 1, a CAD model is introduced in order to find the actual resistance of the coil. To find the total resistance of a single coil, the actual length of winding needs to be found. Through calculations with the help of the 3D CAD model, it could be readily found that the total length of wire in one single coil is $l_{total} = 12346.9\,\mathrm{mm}$. Substitute the value of l_{total}, i.e. l_w, into (3) and the resistance of one single winding could be found, which is $R_w = 55.7\,m\Omega$.

D. Compare the analytical result and that calculated using the measured voltage and current reported from FEM model

It can be seen that the resistance that is calculated by analytical method is slightly bigger than that calculated by the measured current and voltage. The probable reason is that the packing factor is different. It can be readily seen the winding material property is the same in the FEMM property option. The electrical conductivity the software uses to calculate the resistance is the same as ours, which is $\sigma = 58\,\mathrm{MS/m}$. However, FEMM uses a unity packing factor (i.e. $k_{PF} = 1$). This should be the reason why we get a different result from our calculations and simulations.

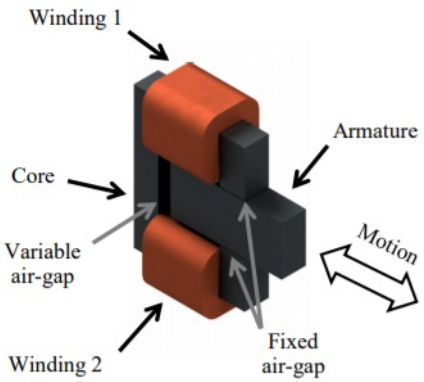

(a) 3-d illustration of the actuator.

Fig. 1. The 3D CAD model of the actuator.

E. Plot the total winding loss as a function of applied current from 0 to 10A

In this case, the current is DC current. Thus, we may consider the resistance to be constant when the current I range from $0\,A$ to $10\,A$. With the intention of finding the most accurate result, it is appropriate to use the resistance calculated using CAD model, which is $R_w = 55.7\,m\Omega$. The power loss in winding is governed by (4). It is readily to use MATLAB to plot the total winding power loss as shown in Fig. 2.

$$P = I^2 R \tag{4}$$

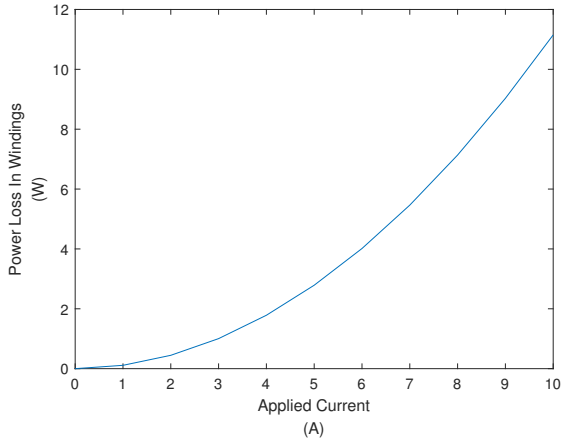

Fig. 2. Total windings (including all 2 windings) Power Loss P v.s. Applied Current I ranging from 0A to 10A.

III. Winding Inductance

In this section, only the half-side inductance is considered because the same turns of coil and current on each side sets up the same magneto-motive force, hence the performance of both sides are symmetrical. The figures of 2D model of the actuator is depicted in Fig. 3 and equivalent magnetic circuit is depicted in Fig. 4

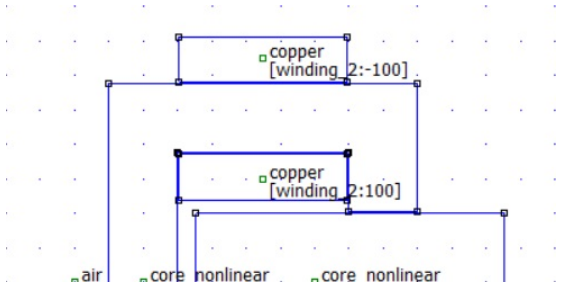

Fig. 3. The half-side actuator from FEMM.

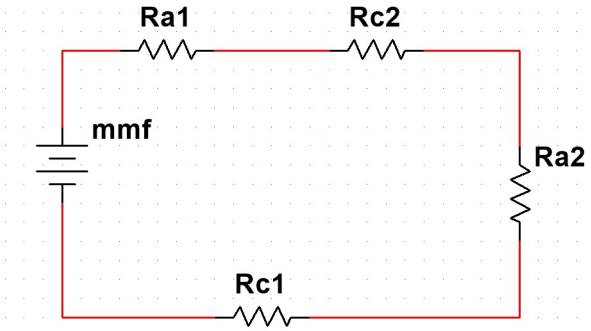

Fig. 4. The half-side actuator equivalent circuit from FEMM.

In this scenario, R_{a1} is the reluctance of the air-gap between the stator core and the armature on the left-hand-side of Fig. 3, R_{a2} is the reluctance of the air-gap between armature and core on the right handside of Fig. 3, R_{c1} is the reluctance of the half-side core and R_{c2} is the reluctance of the half-side armature. The magnetomotive force is generated by 100 turns of coil and 10A current. Assuming the displacement from the original position of the armature is x, then the length of the air-gap is also x.

From the 2D model of the actuator, some required values that are measured by FEMM are described as follows.

The flux length of the half-side stator coil:

$$l_{c1} = 150mm \tag{5}$$

The flux length of the affected half-side armature:

$$l_{c2} = (70 - x)mm \tag{6}$$

The flux length of air-gap on the left:

$$l_{a1} = 0.5mm \tag{7}$$

The flux length of air-gap on the right:

$$l_{a2} = x \quad mm \tag{8}$$

The effective gap area of linear condition:

$$A = 400mm^2 \tag{9}$$

The reluctance is defined as (10), where l is the path length μ_0 is the vacuum permeability, μ_r is the relative permeability and A is the surface.

$$R = \frac{l}{\mu_0 \mu_r A} \tag{10}$$

Then the reluctances of the linear condition could then be found as below.

$$R_{a1} = \frac{l_{a1}}{\mu_0 A} = \frac{0.5 \times 10^{-3}}{4\pi \times 10^{-7} \times 400 \times 10^{-6}} = 9.95 \times 10^5 (At/Wb) \quad (11)$$

$$R_{a2} = \frac{x}{\mu_0 A} = \frac{x \times 10^{-3}}{4\pi \times 10^{-7} \times 400 \times 10^{-6}} = 1.99 \times 10^{-6} x (At/Wb) \quad (12)$$

$$R_{c1} = \frac{l_{c1}}{\mu_0 \mu_r A} = \frac{150 \times 10^{-3}}{4\pi \times 10^{-7} \times 1000 \times 400 \times 10^{-6}} = 2.98 \times 10^5 (At/Wb) \quad (13)$$

$$R_{c2} = \frac{l_{c2}}{\mu_0 \mu_r A} = \frac{(70 + x) * 10^{-3}}{4\pi \times 10^{-7} \times 400 \times 10^{-6}} = (1.39 \times 10^5 + 1.99 \times 10^3 x)(At/Wb) \quad (14)$$

And the summation of all reluctances is

$$\Sigma R = R_{a1} + R_{a2} + R_{c1} + R_{c2} = (1.432 \times 10^6 + 1.99 \times 10^6 x)(At/Wb) \quad (15)$$

The relation between inductance and reluctance is governed by

$$L = \frac{N^2}{\Sigma R} \quad (16)$$

By substituting total reluctance (15) into (16) we can get the inductance when the air-gap fringing is negligible.

$$L = \frac{10^4}{1.432 \times 10^6 + 1.99 \times 10^6 x} (H) \quad (17)$$

As for the scenario when accounting for air-gap fringing flux, using the effective air-gap model that given in [7].

$$A_{eff} = (W + 2g)(T + 2g) = (20 + 2x)(20 + 2x) \quad (18)$$

By replacing A with (18), the reluctances considering the air fringing could be calculated as in (19).

$$R_{a1} = \frac{l_{a1}}{\mu_0 A_{eff}} = \frac{0.5 \times 10^{-3}}{4\pi \times 10^{-7} \times (20 + 1)(20 + 1) \times 10^{-6}} = 9.02 \times 10^5 (At/Wb) \quad (19)$$

$$R_{a2} = \frac{x}{\mu_0 A_{eff}} \quad (20)$$

$$R_{a2} = \frac{10^{-3} x}{4\pi \times 10^{-7} \times (20 + 2x)(20 + 2x) \times 10^{-6}} \quad (21)$$

$$R_{a2} = \frac{7.96 \times 10^8 x}{(20 + 2x)(20 + 2x)} (At/Wb) \quad (22)$$

Then we get the summation of all reluctances, which is shown as in (23).

$$\Sigma R = 1.339 \times 10^6 + 1.99 \times 10^3 x + \frac{7.96 \times 10^8 x}{(20 + 2x)(20 + 2x)} (At/Wb) \quad (23)$$

Hence the inductance considering the air fringing could be calculated by (24).

$$L = \frac{10^4}{1.339 \times 10^6 + 1.99 \times 10^3 x + \frac{7.96 \times 10^8 x}{(20+2x)(20+2x)}} (H) \quad (24)$$

Using the FEMM model, the inductance of the actuator as a function of armature position for both the $core\_linear$ and $core\_nonlinear$ material cases could be readily found. The four inductance trends is shown in Fig. 5.

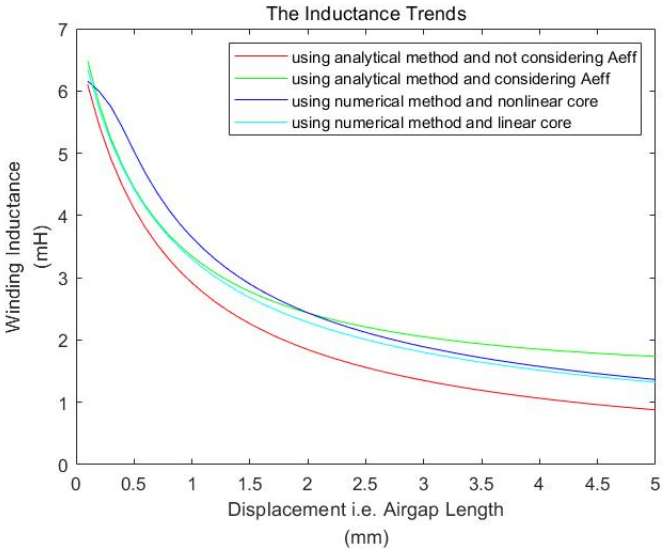

Fig. 5. The inductance trend plotted using four different methods.

From the Fig. 5, it could be found that when the air-gap gets smaller the inductance will increase and slope of the curves will also rise. The reason for that is the inductance is inversely proportional to the reluctance which is proportional to the length of air-gap. Hence, the inductance is reversely proportional to the length of air-gap.

Comparing the trends of the inductance with air-gap considered and without air-gap considered which are the green one and the red one respectively from Fig. 5, it could be found that the curve of the trend of the inductance calculated without considering air-gap fringing is smaller than that calculated with air-gap in that the air-gap induces the effective air-gap area A_{eff} which makes the air-gap area larger. But the differences will get smaller as the air-gap gets smaller. Then a conclusion could be drawn that the air-gap fringing will make a large difference when the air-gap is too large to neglect and vice versa. The inductance trend measured by FEMM using linear core will be compared with that plotted using the analytical method considering the effective air-gap area A_{eff}, because they are both using linear core, the relative permeability μ_r should be the same. Thus, the only difference could be the effective air-gap area A_{eff}. We can see from the Fig. 5, when the air-gap is large, the inductance of the analytical method considering Aeff is larger than the numerical method either using linear core or using

nonlinear core as the result of the fact that the effective air-gap area A_{eff} is not accurate. The effective air-gap area A_{eff} is calculated by using the formula described in (18), which is only an approximate of the real effective air-gap area A_{eff}. Due to the fact that the inductance calculated by our analytical method is slightly bigger than the real one, it could be readily seen that the effective air-gap area A_{eff} calculated is slightly bigger than the one in reality since inductance L is proportional to the effective air-gap area A_{eff}. That is the reason why when the air-gap is large, the inductance calculated using the analytical method considering Aeff is larger than the numerical ones while the linear core and nonlinear core have the same performance.

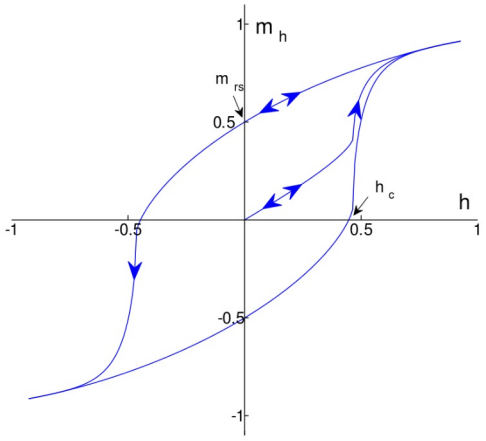

Fig. 6. The B-H curve and hysteresis loop of the nonlinear ferromagnetic material

When the air-gap length is decreasing, it could be seen that the numerical-linear-core curve is drawn closer to the analytical-method-considering-Aeff one. This is because as the reluctance decreasing, the effective air-gap area A_{eff} is getting more accurate. As for the nonlinear one, while the air-gap length becomes smaller, which is between 0.25mm to 5mm, Thus, the relative permeability of the nonlinear core μ_r gets larger as the slope of B-H curve increases. Hence its inductance is higher than the linear one during the period when air-gap is between 0.25mm and 5mm.

Nevertheless, it could be found that when the air-gap is smaller than about 0.4mm, the slope of the inductance trend with a nonlinear core is slower and finally the inductance becomes smaller than the analytical and the linear one. This is because the nonlinear gets saturated, in other words, the relative permeability μ_r decreases, when the flux density gets higher Fig. 6. From the equation (27), because the slope of B-H curve, which is equal to permeability, is getting smaller than the relative permeability plummets. Hence the inductance is also smaller compared with the other two curves.

$$B = \mu_0 \mu_r H \tag{25}$$

IV. Simplified Circuit Model for Nonlinear Core

Based on the previous analysis, the analytical method could not be used to model the actuator with a nonlinear core material [2]. In order to solve this problem, Simulink is used to build a equivalent circuit for the nonlinear core. The equivalent circuit model for nonlinear core could be built using a nonlinear resistance. In this scenario, the current controlled resistor is introduced so that the relation between B and H could be found, which is the same as the voltage-current relation in the equivalent circuit. Based on the equation described in (27), let's assume that the current I corresponds to magnetic flux φ and that voltage U corresponds to magneto-motive force NI. Thus, the equation described in (27) could be transformed in to following equations.

$$\frac{\varphi}{S} = \mu_0 \mu_r \frac{NI}{l} \tag{26}$$

$$NI = \frac{l}{\mu_0 \mu_r(\varphi) S} \cdot \varphi \tag{27}$$

The equation in (27) is in line with the equation in (28).

$$U = R(I) \cdot I \tag{28}$$

In the light of this, a model could be built in Simulink with the *Simscape* tool box [8], which is shown in Fig. 7.

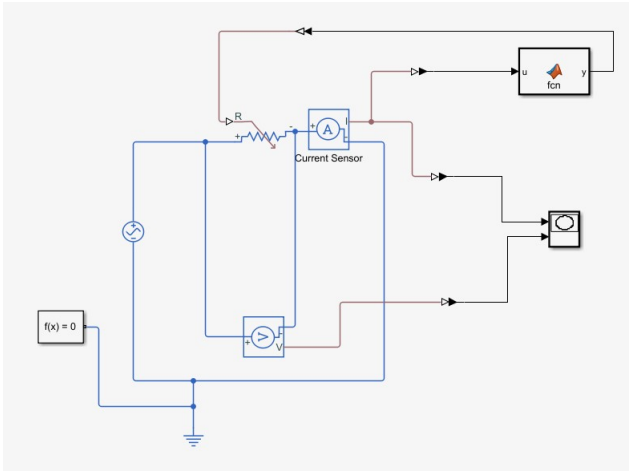

Fig. 7. Simulink model for the equivalent circuit of the nonlinear core.

As shown in Fig. 7, a current controlled resistor is used to emulate the behaviour of a nonlinear core. It is critical to decide the resistance R function w.r.t current I. In the light of [9], the relation between B and H in nonlinear scenario could be define as (29).

$$B = B_{sat} \cdot tanh(a \cdot H) \tag{29}$$

where $B_{sat} = 1.5$, $a = tanh^{-1}(0.5) \cdot \frac{\mu_0 \mu_r}{0.75}$. Thus, the derivative of magneto-motive force NI w.r.t the magnetic flux φ could be found, which is governed by (30).

$$\frac{dNI}{d\varphi} = \frac{d}{d\varphi}\left[\frac{l}{a}tanh^{-1}(\frac{\varphi}{s\cdot 1.5})\right] = \frac{l}{a}\cdot\frac{1}{1-((\frac{\varphi}{1.5S}))^2} \quad (30)$$

Then, all the parameters and formulae could be fed into MATLAB and a B-H curve could be generated through a x-y scope [9], as shown in Fig. 8. It could readily be seen that the BH curve is linear when M.M.F NI is not greater than 40. If M.M.F NI goes greater than 40, the nonlinear characteristic of nonlinear core is shown as these curves. In addition, the parameters used in this example could be altered easily in order to apply to different demands.

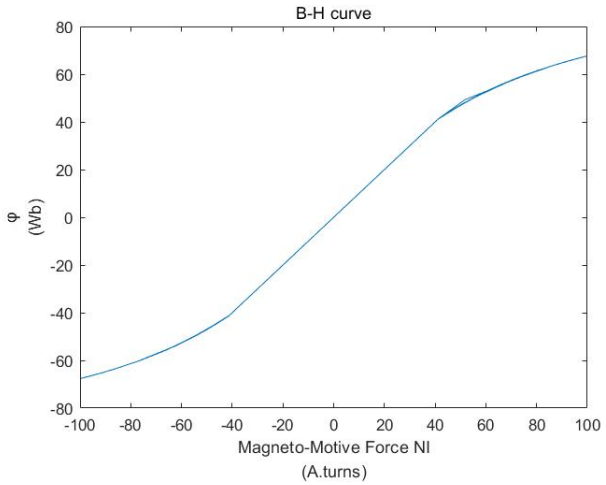

Fig. 8. B-H curve plotted using Simulink and MATLAB.

V. Force on the Armature

If not specified, the following calculations and measurements are all based on the assumption that only one single winding is considered.

A. Using FEMM method to find the $\psi - I$ relation

It could be easily seen that the force varies as the mover of the actuator moving from the closed position to the open position. In order to take the advantage of the actuator, it is critical to find how force varies when the mover is changing its position. The force could be assessed through an energy conservation perspective. The relation between force imparted on the mover and the displacement of the mover is governed by (31) [1]

$$\Delta E_{mech} = \int_{dx_0}^{dx_c} F\mathrm{d}x \quad (31)$$

In order to find the relation between force imparted on the mover and displacement of mover, the difference of mechanical energy ΔE_{mech} must be found. From the conclusion derived in [2], it could be readily found that the difference of Coenergy is the mechanical energy ΔE_{mech} that is looked for, which could be seen from the $\psi - I$ diagrams. Take Fig. 9 as an example, the $\psi - I$ relation is governed by (32).

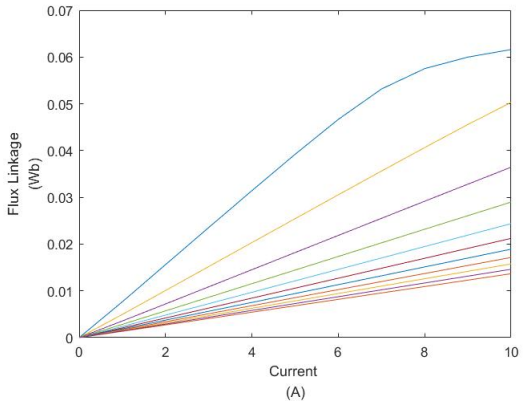

Fig. 9. $\psi - I$ plot with nonlinear core in 10 different positions.

$$F = \frac{\Delta E_{mech}}{\Delta x} \quad (32)$$

It could also be seen in Fig. 9 that the difference of mechanical energy could be calculated by the area encircled by two corresponding curves. Therefore, we could just calculate the area between two curves in order to know the value of the force. However, it is also critical to decide the value of displacement difference dx intending to find the correct value of force F. From the perspective of calculus, the smaller the difference of displacement is, the more precise the value of the force will be. As attested by this, the Fig. 10 shows the $\psi - I$ relation with 50 positions (i.e. air-gap length) ranging from 0.1mm to 5mm with the interval of 0.1mm.

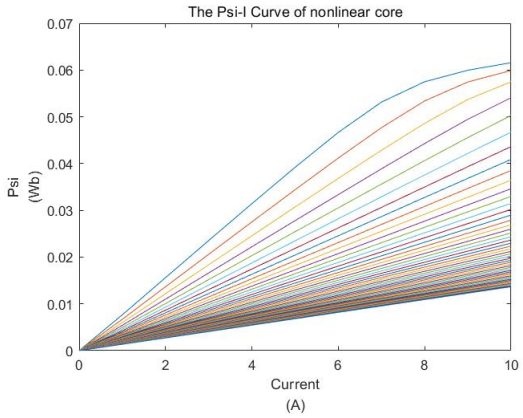

Fig. 10. $\psi - I$ plot with nonlinear core in 50 different positions using FEMM method.

Similarly, the $\psi - I$ relation of the linear core scenario could be found as Fig. 11.

B. Using analytical method to find the $\psi - I$ relation

The same method could also be used in finding the $\psi - I$ relation using the analytical method. The inductance of one single winding considering the effective air-gap area A_{eff} is governed by (24), while the one not considering the effective air-gap area is subject to (17). With the previous

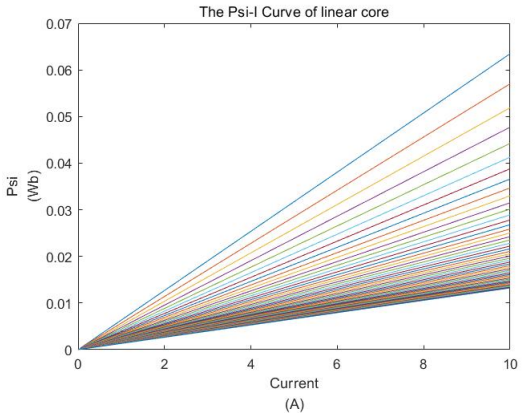

Fig. 11. $\psi - I$ plot with linear core in 50 different positions using FEMM method.

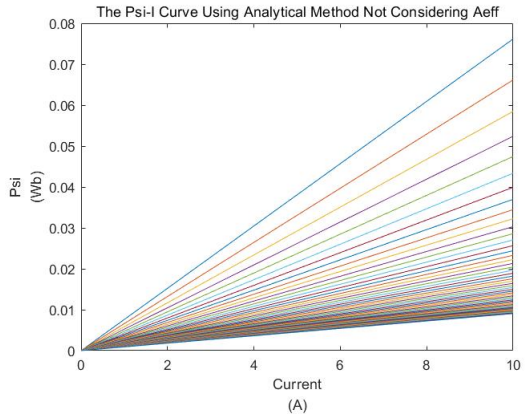

Fig. 13. $\psi - I$ plot considering effective air-gap area A_{eff} in 50 different positions using analytical method.

two equation described in (17) and (24), it could be readily to plot the $\psi - I$ relation considering the effective air-gap area A_{eff} and the one not considering the effective air-gap area A_{eff}. As said previously in this article, with the intention of finding as accurate the force as possible, more position of armature is needed. In the figure drawn using MATLAB, 50 positions (i.e. air-gap length) are evaluated ranging from 0.1mm to 5mm with an interval of 0.1mm. Fig. 12 depicts the $\psi - I$ relation considering effective air-gap area A_{eff} using analytical method. Fig. 13 depicts the $\psi - I$ relation without considering effective air-gap area A_{eff} using analytical method.

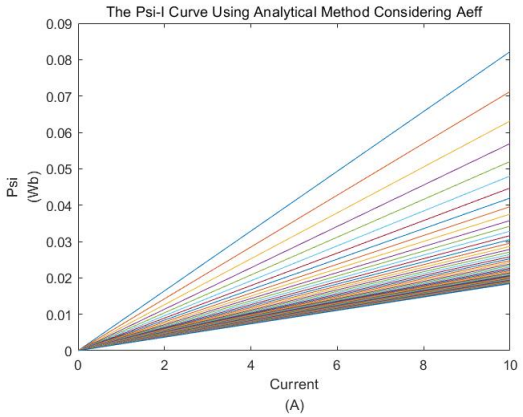

Fig. 12. $\psi - I$ plot considering effective air-gap area A_{eff} in 50 different positions using analytical method.

C. Compare four $\psi - I$ figures plotted with different conditions

It could be seen that the inductance which is the slope of the $\psi - I$ in Fig. 12 where the effective area A_{eff} is considered is slightly smaller than that in Fig. 13 where A_{eff} is not considered. The reason for this is that, in the light of (18), if A_{eff} is considered, A_{eff} should be slightly bigger than A. Thus, the reluctance whose definition is defined in (10) will be slightly smaller in that A_{eff} is considered. The relation between reluctance and inductance is defined in (16). It could be readily found that smaller reluctance results in greater inductance. Thus, we will have bigger slope when A_{eff} is considered. which is corresponding to what we have in Fig. 12 and Fig. 13. However, we can see from the Fig. 10 and Fig. 11 that if FEMM is used to simulate the actuator, the inductance measured by FEMM is smaller than both cases where we use analytical method. Probable 2 reasons are described as following. One of the reasons might be FEMM have a slightly different and more accurate algorithm for finding A_{eff}, while the formula we used which described in (18) is not as accurate as the FEMM simulation. Another reason for the difference between FEMM method and analytical method might be that when the inductance of the magnetic circuit is calculated, the magnetic circuit analysed is simply cut into half. However, cutting the mover in the middle into half might incur inaccuracy of calculations.

D. Compare the Coenergy measured by two different method

The Coenergy difference could be tabulated so that we could observe the changes more intuitively. It is tabulated as in TABLE I.

It can be seen that the difference between the Coenergy measured using two different method always exists. Thus, it is necessary to decide which one should be used. It is readily to say that the Coenergy measured using Integral method is always more accurate that the other one in that the $\psi - I$ curve of the nonlinear one includes some curving lines, which will incur the inaccuracy if we use trapz function. In conclusion, it is appropriate to use Integral method to find the Coenergy rather than to use the trapz one and the method used in this article is Integral method.

E. Plot force-displacement characteristics governed by four different calculation methods

From the above discussion, it could be readily to use MATLAB to plot the force-displacement characteristics with

Displacement (mm)	Coenergy measured by intergal (J)	Coenergy measured by trapz (J)
0.1	0.033135	0.03017
0.2	0.0266	0.022652
0.3	0.01918	0.016071
0.4	0.013892	0.011983
0.5	0.010519	0.009232
0.6	0.008167	0.007348
0.7	0.006603	0.005968
0.8	0.005444	0.004952
0.9	0.00458	0.00417
1	0.0039	0.003594
1.5	0.002038	0.00193
2	0.001278	0.001225
2.5	0.000877	0.00258
3	0.00193	0.001907
3.5	0.00152	0.001523
4	0.001225	0.00124
4.9	0.000877	0.000909

TABLE I
THE COENERGY MEASURED BY FEMM USING DIFFERENT METHOD WITH NONLINEAR CORE

both two windings being considered, which is shown in Fig. 14

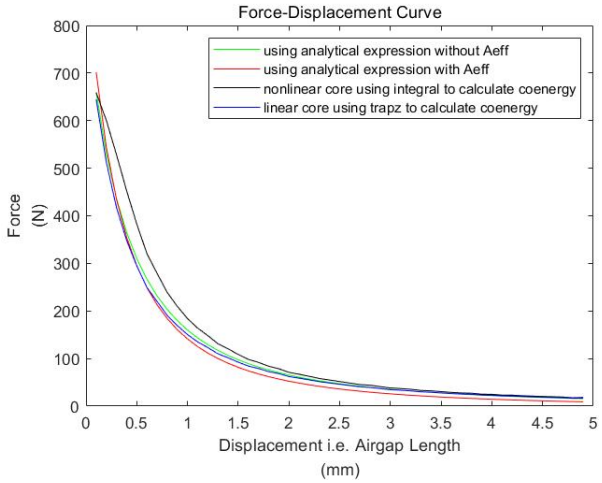

Fig. 14. Force-displacement figure using four different approaches.

When displacement is greater than 2mm three curves stay close to each other except that using analytical method considering Aeff, while the displacement is smaller than 1mm except that using FEMM method with nonlinear core the other three curves stay close to each other. When displacement is close to 0mm, it could be readily seen that there is a saturated phenomenon happens when using FEMM to simulate an actuator with nonlinear core, which is more similar to what will happen in reality. It can be seen that when displacement is greater than 2.5mm, a big difference of the force between the system analyzed by using analytical method considering effective air-gap area A_{eff} and that analyzed by using FEMM with either nonlinear core or linear core. However, the force of that analyzed by using analytical method without considering effective air-gap area A_{eff} is quite similar to that from FEMM simulation. This probably indicates the magnetic flux fringing did not happen in our simulation. Thus, it might be inappropriate to introduce effective air-gap area A_{eff} into our calculations. Furthermore, the reason why the equation we are using to calculate the effective air-gap area A_{eff} is inaccurate is that FEMM is a 2D modelling tool, while our equation seems to apply to the 3D scenario. In addition, when the actuator is split into two parts, the result might be inaccurate because of using the wrong effective air-gap area A_{eff}. Therefore, FEMM itself might be not accurate enough while dealing with the 3D model in a 2D simulation environment. Due to the force-displacement curves, this actuator could be used in electric lock systems [10].

VI. SMART MESHING AND REFINEMENT ALONG THE DESIGNATED SEGMENTS

It could be seen that when using FEMM for simulation, the user needs to specify whether they want to use segment meshing to increase the meshing quality in order to achieve finer calculation results. The meshing option could be found in the FEMM interface or set by MATLAB code. In the normal operation mode, as shown in Fig. 15, it can be seen that the meshing grid in the red circle is quite sparse, while with segment meshing is fully applied, as shown in Fig. 16, the meshing grid in the red oval is relatively abundant which means the calculation resolution is going to be higher and more refined details will be provided. In addition, the meshing elements are recorded in TABLE II.

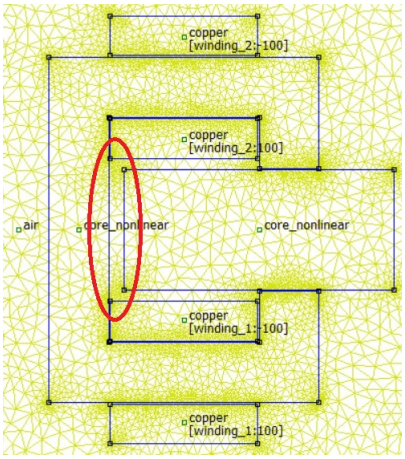

Fig. 15. FEMM model meshed without segment meshing option.

However, higher density of meshing grid means longer calculation time. The trade-off between higher precision and long calculation time need to be made. This could be done by setting automesh argument to 1. The figure in Fig. 17 depicts what will happen if automesh is set. Meanwhile, the figure in Fig. 18 describes what will happen if reset automesh. It could be seen that when using automesh, the area becomes more regular, the meshing density becomes lower where there is only one segment and the meshing density is higher where

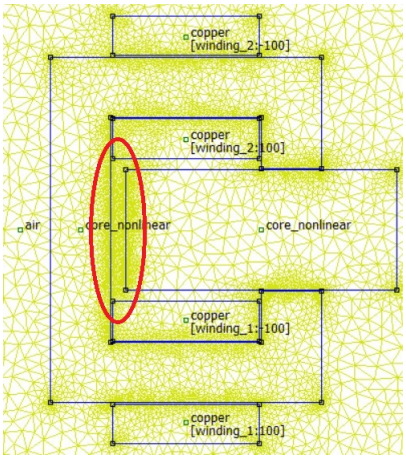

Fig. 16. FEMM model meshed with specific segment meshing option.

there are corners or two segments become close to each other. The reason why the automesh behaves like this is probably that the value analyzed varies little where there is only one segment, while it could vary a lot where there happens to be corner or different segments are close each other, i.e. the discontinuous region. In addition, the edge length is more appropriate than the non automesh one. Thus, higher mesh density could help the users to achieve better observation of these critical areas.

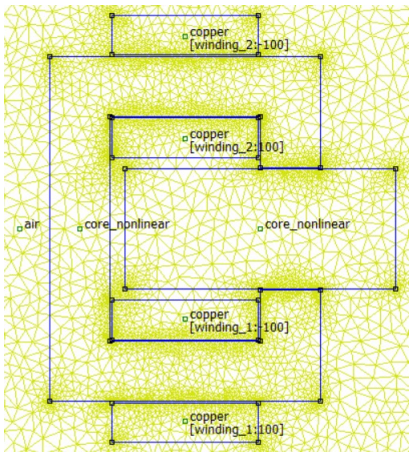

Fig. 17. FEMM model meshed with automesh on.

meshsize	mesh elements
0.9	175918
1	147164
1.1	123216
1.2	108418
1.3	94606
1.4	84812
1.5	77232
automesh	24278
automesh with segment meshing option	26562

TABLE II
THE QUANTITY OF MESHING ELEMENTS MEASURED IN DIFFERENT MESHING CONFIGURATION

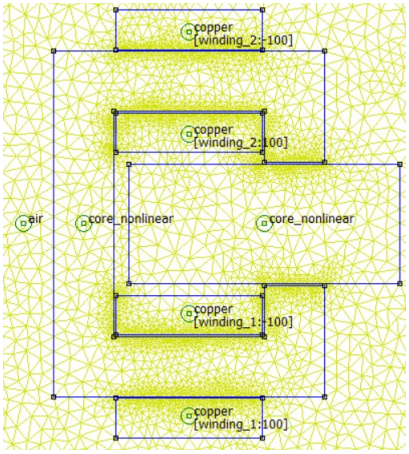

Fig. 18. FEMM model meshed with automesh off.

VII. Conclusion

In the case of modeling and analyzing an actuator, it could be seen that there is nonnegligible difference between the result found by using analytical method and the result measured by using FEMM method. When using analytical method to solve the problem, the saturation and the accurate fringing effect (i.e. effective air-gap area) may not be taken into account. On the other hand, when using FEMM method with a linear core model, the saturation effect cannot be seen in the result. If saturation is not considered, when the air-gap length is very small, the force might be smaller compared to what is actually on the mover in reality. If fringing effect is not considered or it is calculated wrongly, the final force value might be inaccurate. Obviously, the conclusion can be drawn that FEMM gives more accurate results. FEMM is a good tool for analyzing electro-magnetic system in that it could take into account the saturation of the core, the actual effective air-gap area and fringing effect, which is difficult to deal with using analytical method. FEMM uses Finite-Element analysis to find the result which is the closest to the one in reality among all methods and satisfies higher precision demands. However, FEMM itself has its own limitation. FEMM could not give accurate result when dealing with a 3D model as discussed in resistance calculations. Thus, a simulation which support 3D model might be more appropriate to solve this sort of issues. For instance, NEC, HFSS, COMSOL Multiphysics and so on are all software recommended for 3D electromagnetic simulation [11].

[1] [2] [3] [4] [5] [6] [7] [8] [9] [10] [11]

References

[1] B. Suzuki, "Electromagnetic actuators," https://www.electronicshub.org.

[2] N. Simpson, "Electromagnetic characterisation of a short-stroke ferromagnetic actuator: Part b," p. 8, 2020.

[3] C. Lobos, Y. Payan, and N. Hitschfeld, "Techniques for the generation of 3d finite element meshes of human organs," *Informatics in Oral Medicine: Advanced Techniques in Clinical and Diagnostic Technologies*, 11 2009.

[4] E. Dhull, "The role of finite element method in civil engineering," *International Journal of Recent Advances in Science and Technology*, vol. 5, 09 2018.
[5] E. Strømmen, *The Finite Element Method in Dynamics*, 01 2014, vol. 2, pp. 161–204.
[6] N. Simpson, "Electromagnetic characterisation of a short-stroke ferromagnetic actuator: Part a," p. 10, 2020.
[7] N. Simpson and D. Drury, "Electro-mechanical energy conversion," 2020, lecture Notes.
[8] M. Company, "Simscape model and simulate multidomain physical systems," https://uk.mathworks.com/products/simscape.html.
[9] MathWorks, "Simscape electrical technical note," 2020.
[10] S. Clark, "Actuator lock mechanism analysis," 02 2006.
[11] Wikipedia, "Comparison of EM simulation software," https://en.wikipedia.org/wiki/Comparison_of_EM_simulation_software.